Near-Infrared Autofluorescence in Choroideremia: Anatomic and Functional Correlations

JOHANNES BIRTEL, ANNA PAOLA SALVETTI, JASLEEN K. JOLLY, KANMIN XUE, MARTIN GLIEM, PHILIPP L. MÜLLER, FRANK G. HOLZ, ROBERT E. MACLAREN, AND PETER CHARBEL ISSA

• PURPOSE: To investigate near-infrared fundus autofluorescence (NIR-AF) characteristics in patients with choroideremia and to correlate these with anatomic and functional parameters.

• DESIGN: Retrospective, observational case series.

• METHODS: In this multicenter study, 43 consecutive choroideremia patients (79 eyes) underwent multimodal retinal imaging, including near-infrared fundus autofluorescence (NIR-AF), blue autofluorescence (B-AF), optical coherence tomography (OCT), fundus photography, and functional testing including fundus-controlled microperimetry.

• RESULTS: All eyes could be categorized into 3 groups based on patterns of NIR-AF over the island of surviving retinal pigment epithelium: Group 1 (preserved NIR-AF centrally), Group 2 (only disrupted NIR-AF), or Group 3 (absence of NIR-AF). Group 1 eyes showed areas of NIR-AF that matched the areas of B-AF islands ($R^2 = 0.94$, slope 0.84 ± 0.04) while Group 2 eyes showed significantly smaller areas of NIR-AF compared with B-AF ($R^2 = 0.08$; slope 0.02 ± 0.01). The 3 groups differed significantly in terms of residual B-AF island size ($P < .0001$), length of foveal ellipsoid zone ($P = .03$), foveal thickness ($P = .04$), and foveal sensitivity ($P = .01$). Visual acuity ($P = .07$) and central retinal thickness ($P = .06$) did not differ statistically. The length of the ellipsoid zone line was similar to the horizontal diameter of NIR-AF in Group 1 ($R^2 = 0.97$, slope 0.96 ± 0.04), while Group 2 eyes showed broader ellipsoid zone than NIR-AF ($R^2 = 0.60$, slope 0.19 ± 0.03).

• CONCLUSIONS: Choroideremia patients can be stratified into 3 groups based on NIR-AF imaging, which showed morphologic and functional changes correlating with different stages of retinal pigment epithelium degeneration. NIR-AF could be a marker for disease staging in choroideremia, and could be used for patient selection or as an outcome parameter in interventional trials. (Am J Ophthalmol 2019;199:19–27. © 2018 Elsevier Inc. All rights reserved.)

AJO.com Supplemental Material available at AJO.com.

Accepted for publication Oct 16, 2018.

From the Department of Ophthalmology (J.B., M.G., P.L.M., F.G.H., P.C.I.) and Center for Rare Diseases Bonn (ZSEB) (J.B., M.G., P.L.M., F.G.H., P.C.I.), University of Bonn, Bonn, Germany; and Oxford Eye Hospital, Oxford University Hospitals NHS Foundation Trust, and Nuffield Laboratory of Ophthalmology, Nuffield Department of Clinical Neurosciences, University of Oxford, Oxford, United Kingdom (A.P.S., J.K.J., K.X., M.G., R.E.M.,P.C.I.).

Inquiries to Peter Charbel Issa, Oxford Eye Hospital, John Radcliffe Hospital, Oxford OX3 9DU, United Kingdom; e-mail: study-enquiry@outlook.com

CHOROIDEREMIA (CHM; OMIM #303100) IS AN X-linked retinal dystrophy caused by mutations in the *CHM* (or *REP1*) gene.[1–4] The clinical course is characterized by progressive degeneration of the retinal pigment epithelium (RPE) and likely secondary degeneration of photoreceptors and choroid.[5] A central retinal island is usually preserved until late in the disease course.

In vivo gene augmentation therapy, in which a normal copy of the *CHM* gene is delivered to RPE cells and photoreceptors by replication-deficient viral vectors, has shown promising results and is currently being further explored in clinical trials.[6,7] A large therapeutic window is known for choroideremia, with often early diagnosis on the basis of a known family history and usually good visual acuity until the retinal degeneration involves the fovea. Thus, anatomic and/or functional outcome measures are essential to identify suitable patients for therapy, to understand disease progression and optimal timing for intervention, and to measure potential therapeutic effects.

Fundus autofluorescence (AF) imaging facilitates noninvasive assessment of retinal degeneration and supports disease diagnosis, characterization, and monitoring. Currently, blue AF imaging (B-AF), using a 488-nm laser excitation light, is most frequently used in clinical routine. Its main fluorophore is lipofuscin contained in RPE cells.[8] Nevertheless, disadvantages of B-AF include intense glare during image acquisition, reduced visualization of the central retina owing to masking by macular pigment, and potential phototoxic effects.[9–11] An alternative AF approach uses a 787-nm near-infrared (NIR) excitation light.[12] The NIR-AF signal is thought to originate mainly from melanin in the RPE cells and, to a varying degree, from melanin in the choroidal layers.[12] It has been proposed for monitoring disease progression and for distinguishing between functional and dysfunctional retina for instance in patients with retinitis pigmentosa.[13] However, up to now NIR-AF is less commonly used in clinical

0002-9394/$36.00
https://doi.org/10.1016/j.ajo.2018.10.021

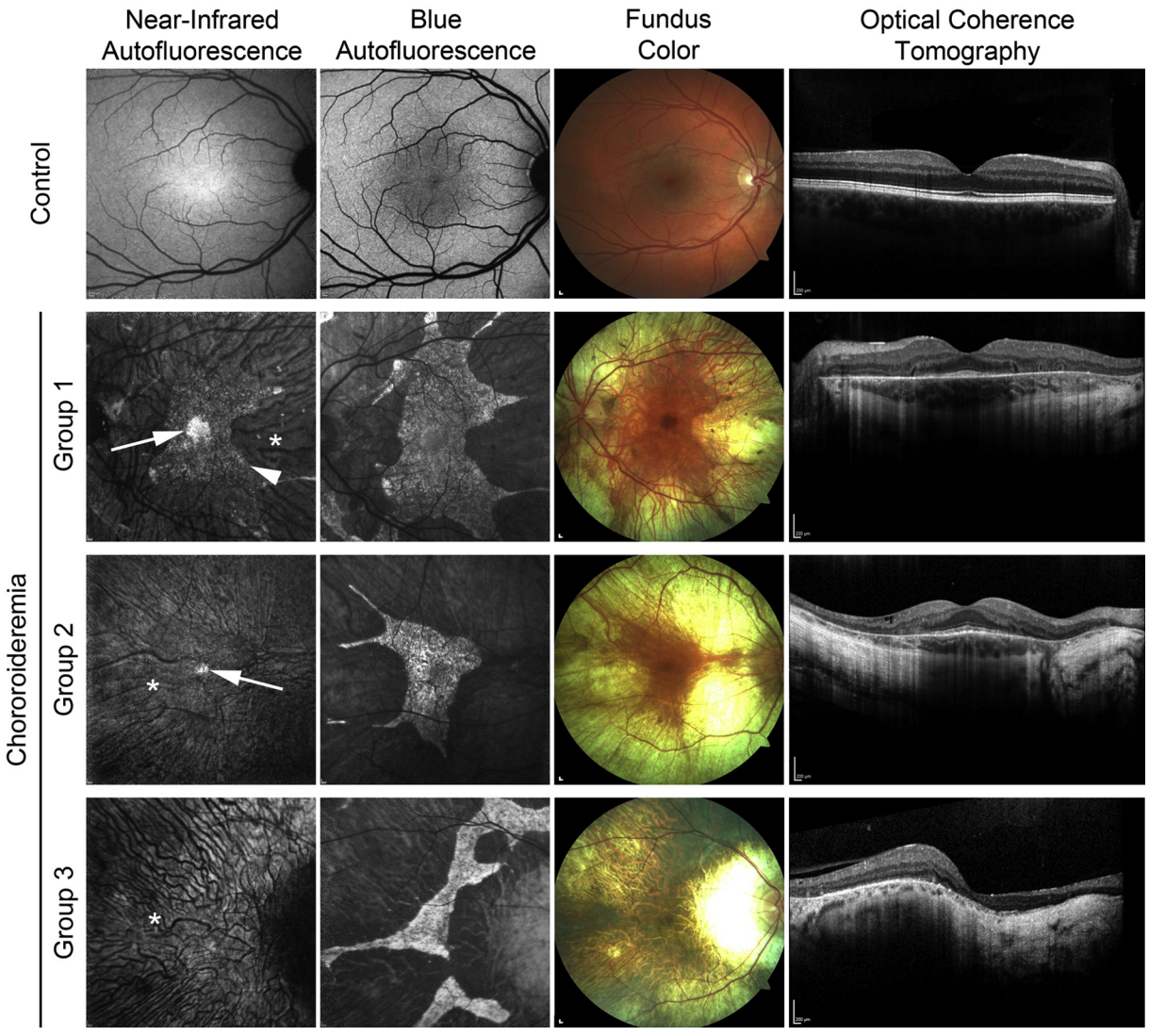

FIGURE 1. Multimodal retinal imaging of a healthy control eye and of choroideremia eyes representing 3 phenotypic groups based on near-infrared autofluorescence (NIR-AF) patterns. A representative example of each group (see Table) is shown. Arrow: pattern A with normal, homogenous NIR-AF; arrowhead: pattern B with granular/mottled NIR-AF; asterisk: pattern C with mainly choroidal NIR-AF.

practice and has not been systematically explored in choroideremia patients.

In this study, we investigated NIR-AF characteristics in a cohort of choroideremia patients; compared NIR-AF, B-AF, and optical coherence tomography (OCT) features; and correlated these to functional parameters. We hypothesize that NIR-AF may have the potential to improve monitoring of disease progression and might be useful as an outcome parameter for treatment trials.

METHODS

• **PATIENTS:** The patients included in this retrospective multicenter study were identified at the Department of Ophthalmology, University of Bonn, and at the Oxford Eye Hospital. Inclusion criteria were (1) the clinical diagnosis of choroideremia and (2) a mutation in *REP1* or a pedigree indicating X-linked inheritance when molecular screening was not performed (n = 4). Eyes with a visual acuity of hand movement or below were excluded from further analysis. The study was in adherence with the Declaration of Helsinki. Institutional review board approval (Ethikkommission, Medizinische Fakultät der Rheinischen Friedrich-Wilhelms-Universität Bonn) and patients' informed consent were obtained. Some of the patients were examined in the context of an ongoing clinical trial (NCT02407678), approved by the UK Health Regulatory Authority (179453).

• **IMAGE ACQUISITION AND ANALYSIS:** All patients underwent a complete ophthalmic examination, including

TABLE. Morphologic and Functional Comparisons of the Identified 3 Groups

	Group 1	Group 2	Group 3	ANOVA (*P* Values)
N (eyes/patients)	34/17	36/20	9/6	
Mean age, y (range)	39 (25–57)	43 (25–73)	38 (27–51)	
NIR-AF patterns	A, B, C (from center outward)	A, C (from center outward)	C	
NIR-AF area[a] (mm^2)[b]	12.58 ± 1.61	0.69 ± 0.06	0	<.0001
B-AF area (mm^2)[b]	14.87 ± 1.75	6.47 ± 0.89	5.78 ± 1.99	<.0001
EZ (μm)[b]	2482 ± 203.8	1963 ± 163.0	1544 ± 218.0	.03
FT (μm)[b]	255 ± 5.5	234 ± 8.7	205 ± 34.8	.04
CRT (μm)[b]	289 ± 5.9	269 ± 7.7	252 ± 25.7	.06
BCVA (logMAR)[b]	0.17 ± 0.02	0.27 ± 0.04	0.26 ± 0.06	.07
Max. LIS (dB)[b]	24.6 ± 0.8	22.8 ± 0.9	18.1 ± 2.9	.01

ANOVA = analysis of variance; B-AF = blue autofluorescence; BCVA = best-corrected visual acuity; CRT = central retinal thickness; EZ = foveal ellipsoid zone; FT = foveal thickness; LIS = foveal light increment sensitivity; NIR-AF = near-infrared autofluorescence.

[a]NIR-AF area included for Group 1 pattern A and B and for roup 2 pattern A.

[b]Mean ± SEM.

logMAR best-corrected visual acuity (BCVA) testing, slit-lamp examination, and funduscopy. Retinal imaging included fundus photography (Visucam; Zeiss, Oberkochen, Germany), spectral-domain OCT and B-AF (both Spectralis HRA+OCT, Heidelberg Engineering, Heidelberg, Germany), and NIR-AF imaging (HRA2; Heidelberg Engineering). For NIR-AF, 787-nm excitation light was used and detected emission light was limited by a barrier filter at 800 nm. For B-AF images, 488-nm excitation light was used and emission was recorded between 500 and 700 nm using barrier filters.

The NIR-AF signal mainly derives from melanin in RPE cells and, to a variable extent, from melanin in the choroid, whereas the B-AF signal is dominated by lipofuscin fluorophores in the RPE.[11,12] On a 30-degree NIR-AF image, the healthy retina is usually characterized by a relatively homogenous autofluorescence that is increased in the fovea owing to its higher RPE melanin density (Figure 1, Top row).[11,14] Loss of the RPE-NIR-AF signal (eg, owing to RPE atrophy) results in better visibility of the fluorescence derived from choroidal melanin. On B-AF, a healthy fundus is also characterized by a mostly homogenous signal; however, the fovea appears darker owing to light absorption by macular pigment and melanin, which both absorb short-wavelength light (Figure 1). In both imaging modalities the blood vessels and the optic disc appear darker owing to light absorption by blood and the absence of a strong fluorophore, respectively.

Residual islands on B-AF[15] and NIR-AF 30-degree images were measured manually by outlining borders using the Heidelberg Eye Explorer software (HEYEX; Heidelberg Engineering). If these areas extended beyond the 30-degree image, a 55-degree image was used instead. To identify the fovea for the measurements of foveal NIR-AF diameters, the fovea was marked on the OCT image and the corresponding mark of the associated NIR reflectance image was overlaid on the NIR-AF image. Furthermore, the software was used to measure the horizontal extent of the foveal ellipsoid zone (EZ, based on single central foveal scan; if the EZ extended beyond the OCT captured area or in case of low-quality OCT images, eyes were excluded), the central retinal thickness (CRT; mean thickness on spectral-domain OCT volume scans within the central 1-mm ETDRS circle), and the foveal thickness (FT; retinal thickness at the foveal center).

• **FUNCTIONAL TESTING:** Retinal sensitivity testing using microperimetry (10-2 threshold test, Macular Integrity Assessment-MAIA; CenterVue, Padova, Italy), which combines scanning laser ophthalmoscopy (SLO) with real-time eye-tracking static perimetry, was performed in all subjects. Owing to the high test-retest variability at the border of retinal degeneration[16] and because of substantial differences in localization and size of the residual island, quantitative analysis of microperimetry data was limited to the test point with highest sensitivity (dB) at or around the fixation point (max. light increment sensitivity).

• **STATISTICAL ANALYSIS:** Statistical analysis was performed using GraphPad Prism v6.0 for Windows (GraphPad Software, La Jolla, California, USA). Areas of preserved RPE on B-AF, BCVA, retinal thickness, and foveal retinal sensitivity were compared among the groups by analysis of variance (ANOVA) test, followed by Tukey test for pair-wise comparison of groups if a significant difference was shown by ANOVA. R^2 was used to evaluate the goodness of fit between the residual area on B-AF and the granular zone G on NIR-AF imaging.[17]

RESULTS

SEVENTY-NINE EYES OF 43 CONSECUTIVE CHM PATIENTS (mean age 41 years, range 25-73 years) were included in

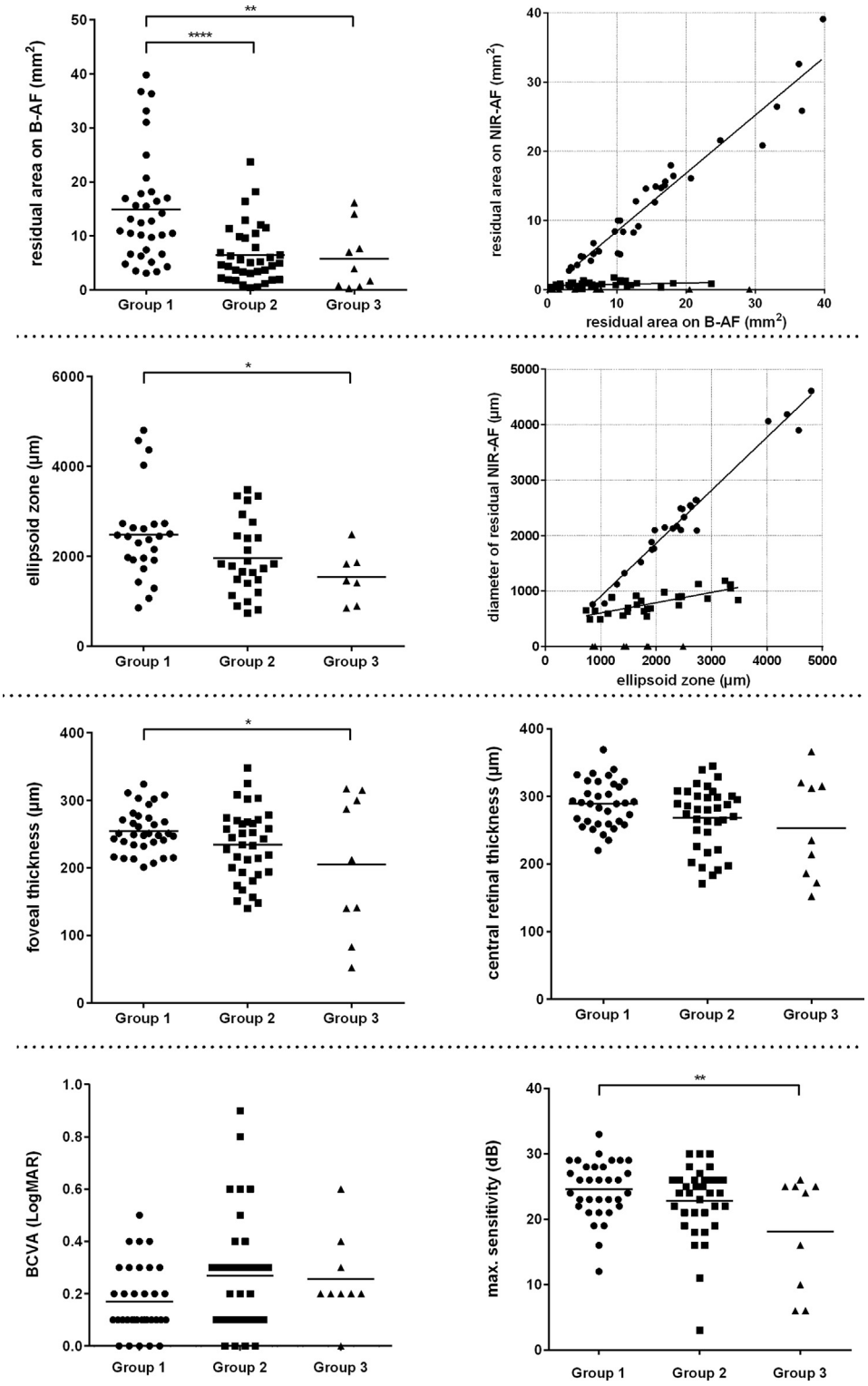

FIGURE 2. Comparison of morphologic and functional parameters between the 3 near-infrared autofluorescence (NIR-AF)-based groups. Differences between groups were identified concerning (Top row) the residual area detected on blue autofluorescence (B-AF) images, (Second row) the length of the visible foveal ellipsoid zone on a horizontal optical coherence tomography scan through the foveal center and its correlation with preserved NIR-AF signal at same position, (Third row) retinal thickness measures, and (Bottom row, right) highest sensitivity around the fixation tested by microperimetry. There was no significant difference in best-corrected visual acuity (BCVA) between groups. *$P < .05$; **$P < .01$, ****$P < .0001$.

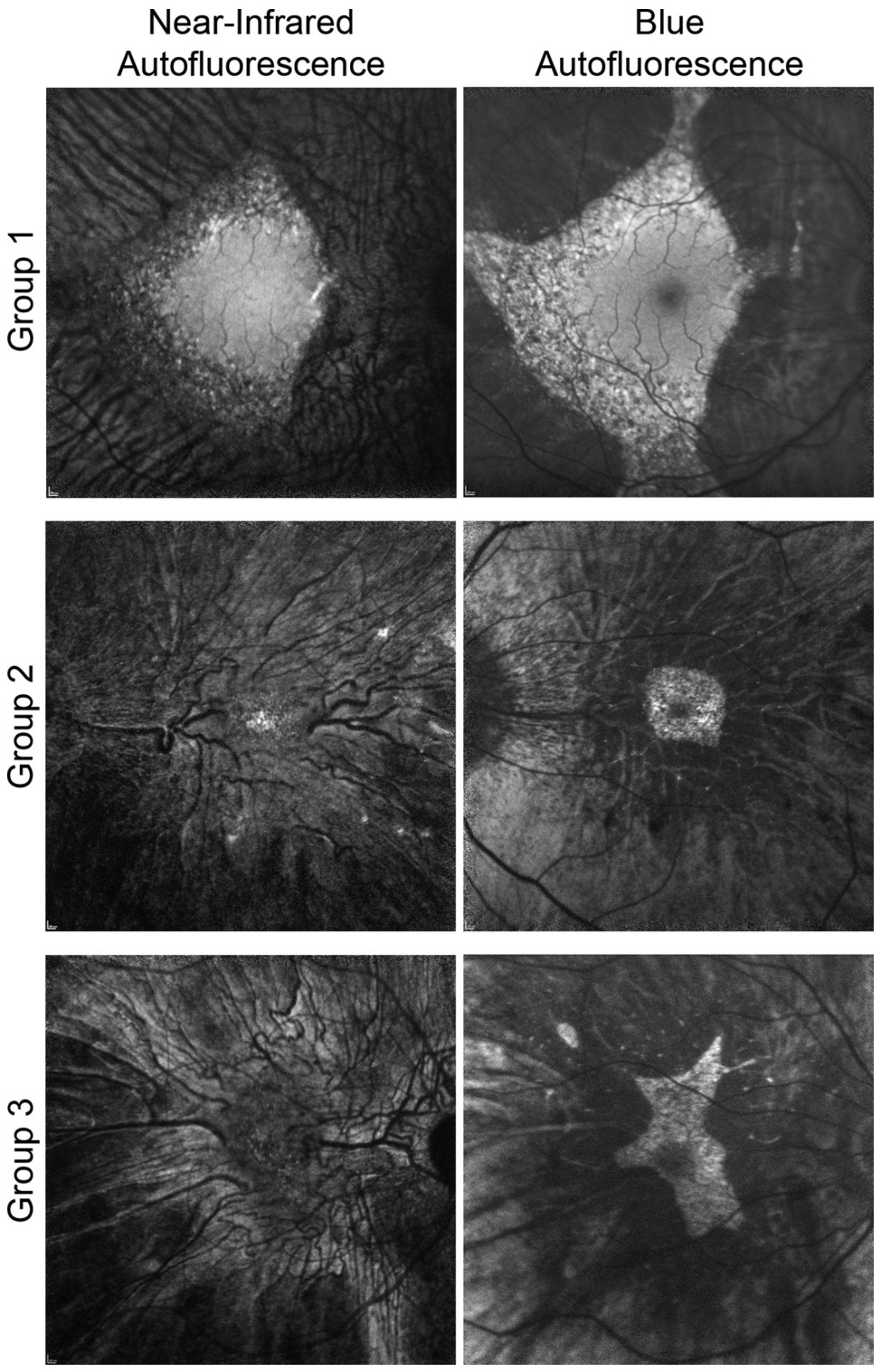

FIGURE 3. Qualitative comparison of blue autofluorescence (B-AF) and near-infrared autofluorescence (NIR-AF) images in choroideremia. In Group 1, both B-AF and NIR-AF images show a well-preserved retinal island of similar size. In more advanced disease, only NIR-AF images reveal whether foveal autofluorescence is preserved (Group 2) or not (Group 3), whereas characteristics of the fovea are masked by macular pigment on B-AF images.

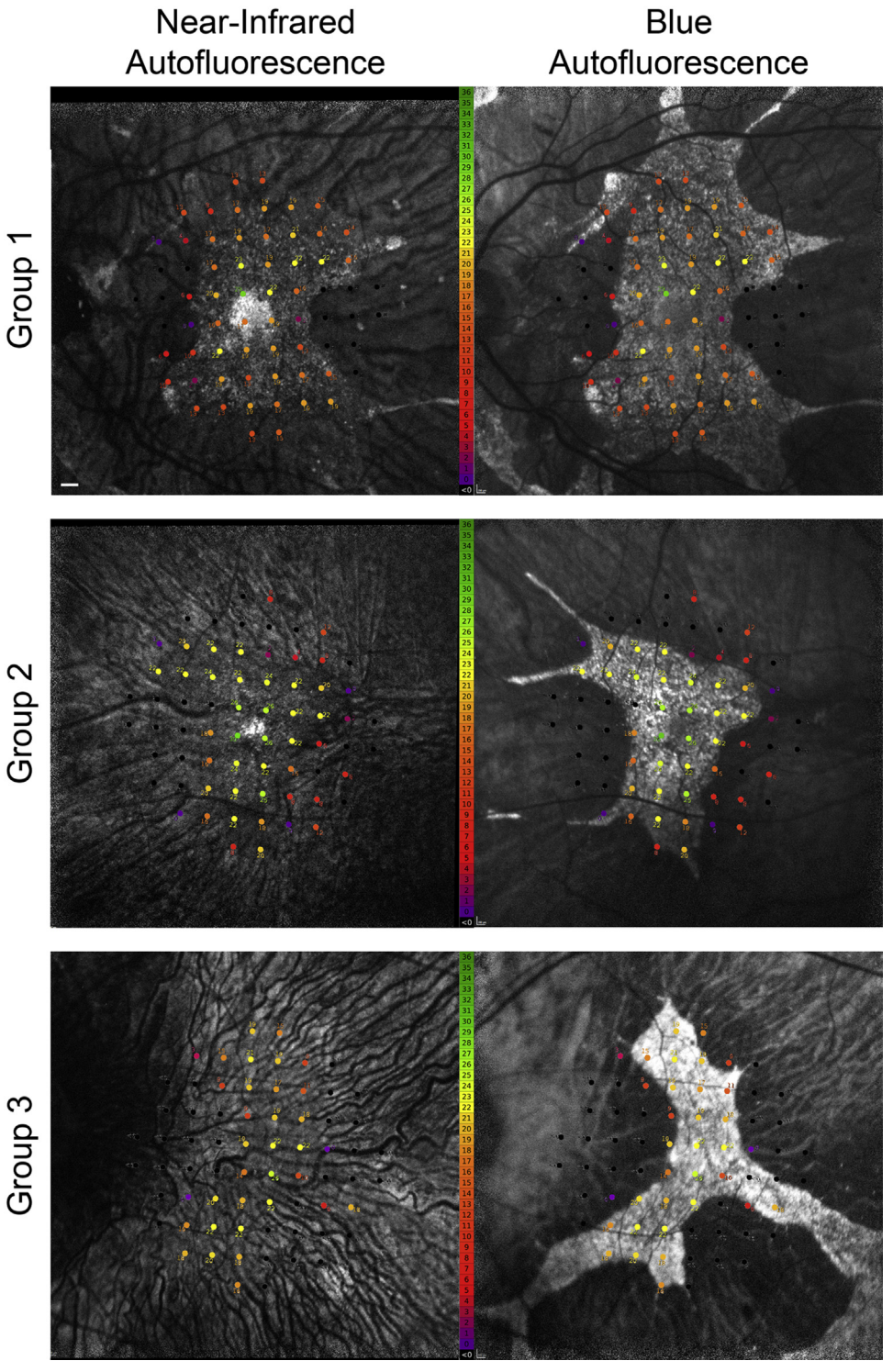

FIGURE 4. Qualitative comparison of macular sensitivity between the 3 near-infrared autofluorescence (NIR-AF) groups. Exemplary cases demonstrate that higher sensitivities measured by microperimetry correlate with a preserved signal on blue autofluorescence rather than on NIR-AF imaging. Loss of NIR-AF seems to precede functional loss on microperimetry testing.

this study. Seven eyes were excluded, owing to either insufficient image quality (n = 4) or low visual acuity (n = 3). The clinical diagnosis of choroideremia was confirmed by genetic testing in 39 patients.

Analysis of NIR-AF images of choroideremia patients revealed 3 distinct local patterns of autofluorescence: areas with homogenous preservation (pattern A, arrows in Figure 1), areas with granular disruption (pattern B,

arrowhead in Figure 1), and areas with complete loss of RPE-derived NIR-AF (pattern C, asterisks in Figure 1). The latter leads to unmasking of underlying choroidal vasculature with low background signal derived from the choroidal stroma. Based on the global composition of these 3 patterns on the NIR-AF image, patients were classified into 3 groups (Figure 1 and Table). Group 1 encompassed patients with patterns A, B, and C demonstrated within a single eye; Group 2 eyes displayed both patterns A and C; and Group 3 eyes only had pattern C visible. Of note, in Group 3 an apparently higher autofluorescence intensity from the choroidal stroma was frequently found. This was most likely the result of increased detector gain in response to very low signal perceived by the camera.

The sizes of autofluorescent islands imaged using NIR-AF and B-AF were significantly different between groups (Table). Pair-wise comparisons revealed significantly larger residual B-AF islands in eyes of Group 1 compared to Groups 2 ($P < .0001$) and 3 ($P = .008$), whereas Groups 2 and 3 were not significantly different (Figure 2, Top row, left). Residual islands on NIR-AF imaging were significantly larger in Group 1 compared to Group 2 ($P < .0001$). In Group 1 eyes, the outer border of pattern B on NIR-AF images approximately matched the outline of the preserved area on B-AF images but was somewhat smaller (slope of regression line 0.84 ± 0.04; $R^2 = 0.94$) (Table, Figure 2, Top row, right). In Group 2 eyes, the definable residual island on NIR-AF images (only pattern A) was typically limited to the fovea and was smaller when compared to the residual island on B-AF images (slope of regression line 0.02 ± 0.01; $R^2 = 0.08$). Qualitative comparison in less advanced cases revealed that areas with normal appearance on B-AF images correlated with pattern A on NIR-AF images (Figure 3, Top row). However, conclusions on the foveal B-AF pattern are usually not possible in more advanced cases owing to the masking effect of macular pigment on B-AF images (Figure 3, Middle and Bottom rows). Thus, presence or absence of preserved foveal NIR-AF signal from the RPE may provide additional information on foveal RPE integrity.

On OCT scans recorded along the horizontal meridian, the length of the visible EZ differed significantly across the 3 groups (Table, Figure 2, Second row, left); pair-wise comparisons revealed significant differences between Groups 1 and 3 ($P = .046$). Eyes were excluded from this analysis if the EZ extended beyond the edge of the OCT image or if the image quality was too poor to delineate retinal layers (n = 9 in Group 1, n = 10 in Group 2, n = 2 in Group 3). In Group 1 eyes, the width of the EZ was similar to the horizontal diameter of the residual NIR-AF island (slope of regression line 0.96 ± 0.04; $R^2 = 0.97$) (Figure 2, Second row, right). Group 2 eyes revealed a wider EZ compared to the diameter of NIR-AF pattern A (regression line 0.19 ± 0.03; $R^2 = 0.60$). Quantitative analysis of foveal thickness revealed a statistically significant difference across the 3 groups; however, pair-wise comparisons revealed significantly thicker measures only for Group 1 compared to Group 3 ($P = .042$). A similar trend of decreasing central retinal thickness from Group 1 to Group 3 did not reach statistical significance (Table, Figure 2, Third row, left and right).

In terms of correlation between the 3 groups and visual function, there was no statistically significant difference in BCVA (Table, Figure 2, Bottom row, left). Moreover, no reliable correlation was found between retinal sensitivity measured by microperimetry and NIR-AF patterns across the whole cohort, partly owing to variability in size and localization of the residual islands (see Methods). In general, the area of preserved retinal function is better represented by the outline of the residual island on B-AF than NIR-AF (Figure 4). However, there appeared to be some correlation between the maximum foveal sensitivity and pattern of residual NIR-AF: the foveal retinal sensitivity was higher in Group 1 patients compared to Group 2 or 3; pair-wise comparisons showed significant difference only between Group 1 and Group 3 ($P = .007$) (Table, Figure 2, Bottom row, right).

DISCUSSION

IN THIS STUDY, WE IDENTIFIED DISTINCT NIR-AF PATTERNS in patients with choroideremia that allowed categorization of eyes into 3 groups. These groups differed with regard to the corresponding residual island size on B-AF imaging, the length of the foveal ellipsoid zone, foveal thickness, and foveal sensitivity. Thus, NIR-AF may serve as an additional imaging parameter for prognosis and monitoring of disease progression.

In all 3 groups the residual island size on NIR-AF was smaller compared to the corresponding areas on B-AF imaging. It has previously been suggested that the main source of NIR-AF is derived from melanin within the RPE, whereas B-AF is mainly derived from lipofuscin within the RPE.[12,18,19] The results of this study suggest that melanin-related AF is lost earlier in the disease course of choroideremia compared to lipofuscin-related autofluorescence. Possible explanations for this observation include early loss of melanin from dysfunctional RPE or changes in the autofluorescence characteristics of melanin.

Presence of the ellipsoid zone and light sensitivity by microperimetry were shown to correlate with the residual island on B-AF imaging.[8] In contrast, the borders of NIR-AF were generally less eccentric compared to the length of the ellipsoid band and loss of sensitivity. Thus, the loss of NIR-AF seems to precede the loss of RPE and photoreceptors at the edge of retinal degeneration. It is possible that the loss of melanin-related NIR-AF represents a specific early stage of RPE alteration in retinal degeneration during which lipofuscin-related B-AF, photoreceptor-related ellipsoid zone, and retinal sensitivity remained preserved. This

assumption is supported by similar findings in rod-cone dystrophies[13] or Stargardt disease,[20] where alterations in NIR-AF also seem to precede those in B-AF. With regard to *REP1* gene augmentation therapy, it could be speculated that eyes with preserved NIR-AF (ie, pattern A) might be more responsive to treatment, given that gene therapy may better rescue RPE cells with early dysfunction than those that have sustained a critical amount of metabolic distress. Hence, patient stratification according to NIR-AF pattern (eg, treating patients with preserved NIR-AF at least in the foveal region) may be of benefit for future clinical trials.

The early loss of melanin-related NIR-AF seen in this study suggests that alterations within RPE cells occur rather early in the disease process. Whether this observation is owing to loss-of-function mutations in *REP1*, which plays a key role in intracellular vesicular trafficking, or if the finding represents a similar (but yet undetermined) pathophysiological event as in other retinal dystrophies, remains unknown.

Visual acuity and central retinal thickness showed no significant differences between the NIR-AF groups. This is perhaps unsurprising given that the fovea is usually the last part of the retina to be encroached by the shrinking edge of degeneration, and choroideremia patients often maintain near-normal visual acuity until the end stage of disease.[15,21,22]

A challenge of NIR-AF imaging is that the signal from the RPE is often low, resulting in poor differentiation of the RPE from the surrounding AF. To achieve greater contrast between RPE and other sources of fluorescence, Cideciyan et al. introduced reflectance-normalized NIR-AF imaging by dividing the NIR-AF signal point-by-point by the corresponding NIR-reflectance image, and showed that these images seemed similar to B-AF images.[11] This type of image processing might be beneficial in more in-depth evaluation of the patterns of NIR-AF in choroideremia, but required standardized images were not available in this project.

Apart from potentially being a more sensitive modality for detecting early RPE alteration than B-AF, NIR-AF holds further advantages over B-AF by avoiding the potential phototoxicity associated with repeated exposure to short-wavelength blue light, particularly when monitoring disease progression in retinal dystrophies.[9,10,23,24] Moreover, NIR-AF imaging provides superior patient comfort and better cooperation, which has particular advantages in children and photophobic patients.[11] And since the foveal NIR-AF signal is not masked by macular pigment as compared to B-AF, NIR-AF facilitates better evaluation of the foveal region, which is functionally vital.[25]

Based on these results, we propose that incorporation of NIR-AF imaging in the evaluation of choroideremia may improve disease monitoring by facilitating the detection of early RPE alterations as part of the natural history of the disease. The classification of eyes based on NIR-AF pattern may help in patient selection and predicting response to potential therapy.

FUNDING/SUPPORT: THIS WORK WAS SUPPORTED BY THE NATIONAL INSTITUTE FOR HEALTH RESEARCH (NIHR) OXFORD Biomedical Research Centre (BRC), United Kingdom; ProRetina Foundation, Germany; and the German Research Foundation (DFG; MG grant # GL920/1-1; PLM grant # MU4279/1-1), Germany. The views expressed are those of the authors and not necessarily those of the NHS, the NIHR or the Department of Health. The sponsor and funding organization had no role in the design or conduct of this research. Financial Disclosures: The following authors have no financial disclosures: Johannes Birtel, Anna Paola Salvetti, Jasleen K. Jolly, Kanmin Xue, Martin Gliem, Philipp L. Müller, Frank G. Holz, Robert E. MacLaren, and Peter Charbel Issa. All authors attest that they meet the current ICMJE criteria for authorship.

REFERENCES

1. van den Hurk JA, Schwartz M, van Bokhoven H, et al. Molecular basis of choroideremia (CHM): mutations involving the Rab escort protein-1 (REP-1) gene. *Hum Mutat* 1997; 9(2):110–117.
2. Cremers FP, Sankila EM, Brunsmann F, et al. Deletions in patients with classical choroideremia vary in size from 45 kb to several megabases. *Am J Hum Genet* 1990;47(4):622–628.
3. Seabra MC, Brown MS, Goldstein JL. Retinal degeneration in choroideremia: deficiency of rab geranylgeranyl transferase. *Science* 1993;259(5093):377–381.
4. Seabra MC, Brown MS, Slaughter CA, et al. Purification of component A of Rab geranylgeranyl transferase: possible identity with the choroideremia gene product. *Cell* 1992; 70(6):1049–1057.
5. Morgan JI, Han G, Klinman E, et al. High-resolution adaptive optics retinal imaging of cellular structure in choroideremia. *Invest Ophthalmol Vis Sci* 2014;55(10):6381–6397.
6. Edwards TL, Jolly JK, Groppe M, et al. Visual acuity after retinal gene therapy for choroideremia. *N Engl J Med* 2016; 374(20):1996–1998.
7. MacLaren RE, Groppe M, Barnard AR, et al. Retinal gene therapy in patients with choroideremia: initial findings from a phase 1/2 clinical trial. *Lancet* 2014;383(9923): 1129–1137.
8. Xue K, Oldani M, Jolly JK, et al. Correlation of optical coherence tomography and autofluorescence in the outer retina and choroid of patients with choroideremia. *Invest Ophthalmol Vis Sci* 2016;57(8):3674–3684.
9. Cideciyan AV, Swider M, Aleman TS, et al. Reduced-illuminance autofluorescence imaging in ABCA4-associated retinal degenerations. *J Opt Soc Am A Opt Image Sci Vis* 2007;24(5):1457–1467.
10. Morgan JI, Hunter JJ, Masella B, et al. Light-induced retinal changes observed with high-resolution autofluorescence imaging of the retinal pigment epithelium. *Invest Ophthalmol Vis Sci* 2008;49(8):3715–3729.

11. Cideciyan AV, Swider M, Jacobson SG. Autofluorescence imaging with near-infrared excitation:normalization by reflectance to reduce signal from choroidal fluorophores. *Invest Ophthalmol Vis Sci* 2015;56(5):3393–3406.
12. Keilhauer CN, Delori FC. Near-infrared autofluorescence imaging of the fundus: visualization of ocular melanin. *Invest Ophthalmol Vis Sci* 2006;47(8):3556–3564.
13. Duncker T, Tabacaru MR, Lee W, et al. Comparison of near-infrared and short-wavelength autofluorescence in retinitis pigmentosa. *Invest Ophthalmol Vis Sci* 2013;54(1):585–591.
14. Weiter JJ, Delori FC, Wing GL, Fitch KA. Retinal pigment epithelial lipofuscin and melanin and choroidal melanin in human eyes. *Invest Ophthalmol Vis Sci* 1986;27(2):145–152.
15. Jolly JK, Edwards TL, Moules J, et al. A qualitative and quantitative assessment of fundus autofluorescence patterns in patients with choroideremia. *Invest Ophthalmol Vis Sci* 2016; 57(10):4498–4503.
16. Dimopoulos IS, Tseng C, MacDonald IM. Microperimetry as an outcome measure in choroideremia trials: reproducibility and beyond. *Invest Ophthalmol Vis Sci* 2016;57(10):4151–4161.
17. Linnet K. Estimation of the linear relationship between the measurements of two methods with proportional errors. *Stat Med* 1990;9(12):1463–1473.
18. Delori FC, Staurenghi G, Arend O, et al. In vivo measurement of lipofuscin in Stargardt's disease–fundus flavimaculatus. *Invest Ophthalmol Vis Sci* 1995;36(11):2327–2331.
19. Sparrow JR, Gregory-Roberts E, Yamamoto K, et al. The bisretinoids of retinal pigment epithelium. *Prog Retin Eye Res* 2012;31(2):121–135.
20. Duncker T, Marsiglia M, Lee W, et al. Correlations among near-infrared and short-wavelength autofluorescence and spectral-domain optical coherence tomography in recessive Stargardt disease. *Invest Ophthalmol Vis Sci* 2014;55(12): 8134–8143.
21. Jolly JK, Xue K, Edwards TL, et al. Characterizing the natural history of visual function in choroideremia using microperimetry and multimodal retinal imaging. *Invest Ophthalmol Vis Sci* 2017;58(12):5575–5583.
22. Heon E, Alabduljalil T, McGuigan ID, et al. Visual function and central retinal structure in choroideremia. *Invest Ophthalmol Vis Sci* 2016;57(9):OCT377–387.
23. Teussink MM, Lambertus S, de Mul FF, et al. Lipofuscin-associated photo-oxidative stress during fundus autofluorescence imaging. *PLoS One* 2017;12(2):e0172635.
24. White DA, Fritz JJ, Hauswirth WW, et al. Increased sensitivity to light-induced damage in a mouse model of autosomal dominant retinal disease. *Invest Ophthalmol Vis Sci* 2007; 48(5):1942–1951.
25. Cideciyan AV, Hufnagel RB, Carroll J, et al. Human cone visual pigment deletions spare sufficient photoreceptors to warrant gene therapy. *Hum Gene Ther* 2013;24(12): 993–1006.